Research Article Vol. 59, No. 28 / 1 October 2020 / Applied Optics 8959

applied optics

Ultrashort all-fiber Fabry–Perot interferometer fabricated by a CO_2 laser

Qianqian Zhang,[1] Zhiyuan Fan,[1] Jianping Zhang,[1] Fengbo Zhang,[1] Qiang Zhang,[1,2,3] and Yongmin Li[1,2,4]

[1]State Key Laboratory of Quantum Optics and Quantum Optics Devices, Institute of Opto-Electronics, Shanxi University, Taiyuan 030006, China
[2]Collaborative Innovation Center of Extreme Optics, Shanxi University, Taiyuan 030006, China
[3]e-mail: qzhang@sxu.edu.cn
[4]e-mail: yongmin@sxu.edu.cn

Received 16 July 2020; revised 12 September 2020; accepted 12 September 2020; posted 14 September 2020 (Doc. ID 402999); published 1 October 2020

We proposed and demonstrated a method to fabricate ultrashort all-fiber Fabry–Perot interferometers by splicing a standard single-mode fiber and another single-mode fiber with a concave surface constructed by a CO_2 laser pulse. The geometric parameters of the concave surface could be controlled flexibly by adjusting the laser pulse and the relative position between the laser beam and the optical fiber. In our experiments, the minimum depth of the concave surfaces is 0.12 μm, which offers a means of fabricating an all-fiber Fabry–Perot interferometer with submicrometer cavity length. Moreover, the ultralow-roughness concave surface fabricated by a CO_2 laser pulse is beneficial to improve the fringe visibility of the interferometer. These advantages make it attractive for practical applications.

https://doi.org/10.1364/AO.402999

1. INTRODUCTION

Fiber-optic Fabry–Perot (FP) interferometers have been utilized in various exciting applications [1–6] owing to the prominent advantages of miniature size, resistance to harsh environments, low fabricating cost, and immunity to electromagnetic interference. Compared with FP interferometers based on hybrid materials, all-fiber FP interferometers are more suitable for the smart structures integrated with the main structure, sensors, and controllers. To construct all-fiber FP interferometers, many artful fabricating techniques have been proposed, e.g., fusion spliced [7–13], focused ion beam milling [14–19], chemical etching [20,21], and laser micromachining [22–24]. Ultrashort all-fiber FP interferometers are promising devices for some applications due to the merits of high sensitivity, large free spectral range, low temperature cross sensitivity, and compact size. For example, when an all-fiber FP interferometer is embedded into smart structures to monitor their strain, the sensitivity of the FP interferometer sensor is inversely proportional to the cavity length of the FP interferometer. For all reported all-fiber FP interferometers [7–28], to the best of our knowledge, the minimum cavity length is about 4 μm. Therefore, it is meaningful to explore new techniques for fabricating FP interferometers with shorter cavity lengths.

In this work, we proved and demonstrated a novel strategy to construct an ultrashort all-fiber FP interferometer by splicing a standard single-mode fiber (SMF) to another SMF with a concave surface on the end face. The concave surface is fabricated by focusing a CO_2 laser pulse on the end face of the SMF. The geometric parameters of the concave surface could be tailored flexibly by adjusting the parameters of the laser pulse and the relative position between the laser beam and end face of the optical fiber. According to the measurement results via atomic force microscopy (AFM), the minimum concave surface depth was 0.12 μm for our experimental setup. Therefore, this method can be utilized to fabricate an all-fiber FP interferometer with submicrometer cavity length. Meanwhile, the roughness of the concave surface fabricated by a CO_2 laser pulse is far lower than that fabricated by a femtosecond laser or focused-ion beam, which is beneficial to improve the fringe visibility of the FP interferometer. Moreover, the cost of the machining system based on a CO_2 laser is far less than that based on a femtosecond laser or focused-ion beam. Owing to these advantages, the proposed method has great prospects in practical applications.

2. FABRICATION AND PRINCIPLE

A. Fabrication of the Concave Surface

The most important work for the proposed FP interferometer is to fabricate a suitable coaxial concave surface on the end face of the optical fiber. A CO_2 laser is an efficient tool for polishing surfaces of silica devices because of strong absorption at 10.6 μm for fused silica [29–31]. By moderating the light intensity,

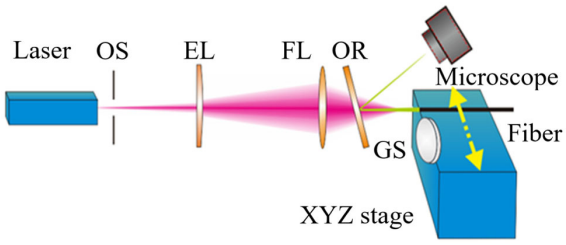

Fig. 1. Experimental system for fabricating the concave on the optical fiber's end face, including an optical shutter (OS), extender lens (EL), focusing lens (FL), optical reflector (OR), glass substrate (GS), optical microscope, and an XYZ stage.

the melt layer on the surface of fused-silica devices could be controlled efficiently. As the intensity increases further, the surface silica on the devices could be evaporated [30,32]. The evaporation technique is promising for constructing concave surfaces on the end face of optical fibers. Therefore, we utilize a CO_2 laser pulse to fabricate grooves on optical fibers in our experiments. The schematic of the machining setup for the concave surface is shown in Fig. 1. The processing setup includes a laser focusing system and an alignment system for precisely locating the optical fiber's position. The CO_2 laser focusing part includes a CO_2 laser (L4S, Access laser), optical shutter, extender lens, and focusing lens; further, the optical fiber alignment part consists of an optical microscope, translation stage (M-562-XYZ, Newport), and optical reflector. Some parameters play key roles in the fabrication of the concave surface, such as laser intensity, number and duration time of the laser pulse, and the distance between the laser beam waist and the end face of the optical fibers. In our experiments, the maximum laser power was 900 mW, and the pulse duration time was from 25 to 50 ms. The distance between the laser beam waist and the end face of the SMF was from 0 to 200 μm.

To fabricate a coaxial concave surface on the end face of the SMF, a glass substrate is used as a positioning reference in our experiments. The fabrication procedure for the concave surface is shown in Fig. 2. First, a glass substrate and an SMF are fixed on the XYZ translation stage, where the surface of the glass

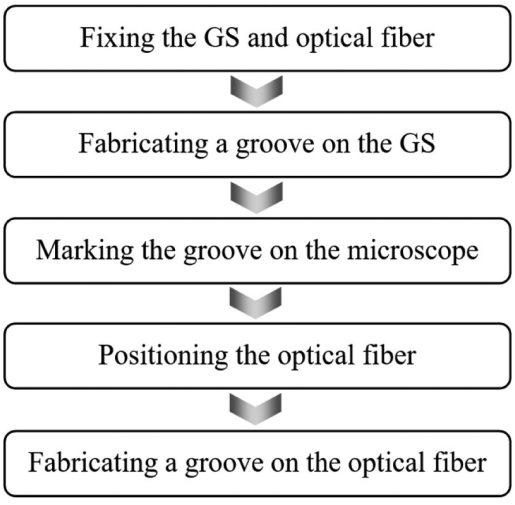

Fig. 2. Fabrication procedure for fabricating the concave on the optical fiber's end face.

substrate and end face of the SMF are coplanar. Second, a groove is fabricated on the glass substrate by adjusting the parameters of the laser pulse and the position of the glass substrate. Third, an optical reflector is inserted between the focusing lens and XYZ translation stage to observe the position of the groove with an optical microscope. The contour of the groove can be marked in the microscope's software to locate the laser beam's position. Then, we align the optical fiber with the groove's reference contour in the optical microscope software to obtain a coaxial groove on the optical fiber's end face. Finally, we could fabricate a suitable concave surface on the end face of the SMF after removing the optical reflector. Here, the geometric parameters of the concave surface could be tailored flexibly by adjusting the laser intensity, duration time and number of the laser pulse, and the relative position between the laser beam and the optical fiber's end face.

In our experiments, we have fabricated a lot of optical fibers with concave surfaces and measured the concave surface profiles with an AFM and optical microscope. Figure 3 provides images of several representative optical fibers with concave surfaces by an AFM and optical microscope. Figures 3(a) and 3(b) show the surface profile and sectional line through the center of the

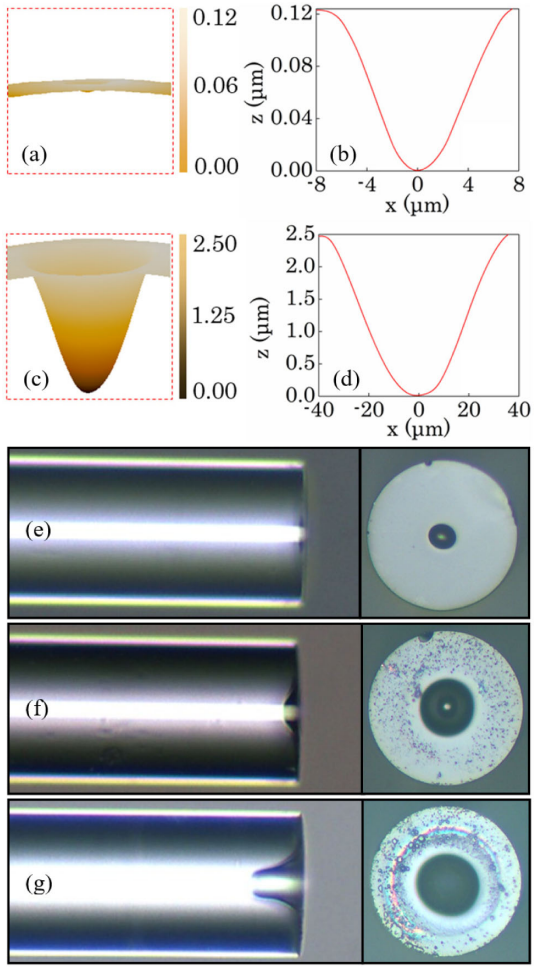

Fig. 3. (a) and (c) Surface profiles of the grooves by an AFM. (b) and (d) Corresponding section lines through the centers of the grooves. (e)–(g) Side views (left) and end faces (right) of the grooves with depths of 2.5, 15, and 50 μm.

groove with 0.12 μm depth and 16 μm width. The depth of the groove could be decreased further by reducing the intensity during time of the laser pulse and increasing the distance between the beam waist and the optical fiber's end face. Therefore, the proposed method paves the way to fabricate an all-fiber FP interferometer with submicrometer cavity length. The AFM images of the groove with 2.5 μm depth and 80 μm width are shown in Figs. 3(c) and 3(d); the corresponding image from an optical microscope is shown in Fig. 3(e). According to the AFM images, the roughness of the concave surface is far lower than that machined by a femtosecond laser or focused-ion beam. The ultralow roughness should owe to the surface tension of the melt layer on the surface of the end face. It has been proved that it is an efficient way to smooth the surface of fused silica using a CO_2 laser [29,30]. A smooth reflector is essential for improving the fringe visibility of the FP interferometer. Figures 3(f) and 3(g) show side views and end faces of the grooves with depths of 15 and 50 μm.

B. Construction of the FP Interferometer

After fabrication of the concave surface on the end face of the optical fiber, it needs to be spliced with a standard SMF to construct an FP interferometer. The arc offset splicing technique is used to ensure the FP interferometer's mechanical strength and reduce deformation of the concave surface morphology according to our previous methods [33]. First, the optimized splicing parameters are obtained by observing the change of grooves with different geometric parameters when an arc is applied to the SMF with a concave surface. Second, an undeformed low-strength splicing joint is formed between the SMF with a concave surface and another standard SMF. Then, the splicing joint is further strengthened by additional small arc discharges. This splicing technique can effectively eliminate the deformation of the concave surface and uncertainty of the cavity length. In the splicing process, an offset of 200 μm is used, and the current and duration time of the arc discharge are 500 and 20 ms, respectively. Figure 4 shows the side views of four representative FP interferometers fabricated by this method, where the depths of grooves on the end faces of the optical fibers are 2.9 (a), 5.1 (b), 10.5 (c), and 15.1 (d) μm, respectively.

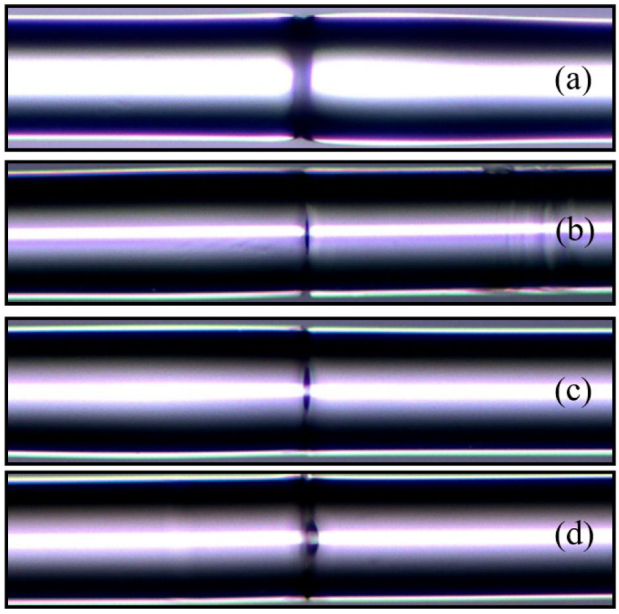

Fig. 4. Images of the FP interferometers with different-depth grooves of (a) 2.9, (b) 5.1, (c) 10.5, and (d) 15.1 μm.

C. Principle of the FP Interferometer

Figure 5 shows a schematic of the FP interferometer. The theoretical model of the proposed FP interferometer is two-beam interference, and the normalized reflective spectrum of the FP interferometer with a cavity length L is

$$I_{FP} = R + (1-a_1)^2\,(1-a_2)\,(1-b)^2(1-R)^2R + 2R\sqrt{1-a_2}\,(1-a_1)\,(1-b)\,(1-R) \times \cos\left(\frac{4\pi nL}{\lambda}+\pi\right), \tag{1}$$

$$R = \left(\frac{n_{\text{fiber}}-n}{n_{\text{fiber}}+n}\right)^2, \tag{2}$$

$$b = \frac{kL}{n}, \tag{3}$$

where R, λ, n, and n_{fiber} are the reflection coefficient, wavelength of input light, refractive indexes of the air and optical fiber; a_1 and a_2 are the losses at the end faces of the two optical fibers (e.g., roughness); k is a constant; and b is the loss resulting from the mode mismatch between the end face of the input optical fiber (left) and reflected light from the other optical fiber (right). According to Eq. (1), rough surfaces of the optical fibers not only result in reduction of fringe visibility but also affect the reflective intensity of the FP interferometers. Therefore, the ultralow roughness of the concave surface fabricated by this method is beneficial to obtain FP interferometers with high visibility and intensity. Meanwhile, the mode-mismatch loss b could be effectively reduced by decreasing the cavity length according to Eq. (3), and the fringe visibility will increase as the cavity length decreases. It should be noted that the cavity length calculated by the common relationship between the free spectrum range and the cavity length is not accurate for ultrashort FP interferometers. According to Eq. (1), the mth dip wavelength λ_{dip} and tip wavelength λ_{tip} of the interference reflective spectra of the FP interferometers is

$$\lambda_{\text{dip}} = \frac{2n}{m}L, \tag{4}$$

$$\lambda_{\text{tip}} = \frac{4n}{2m-1}L. \tag{5}$$

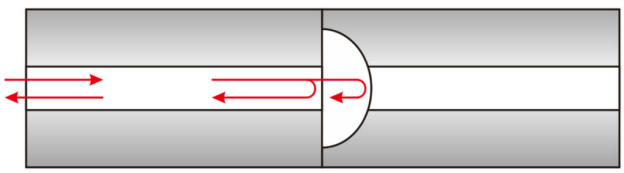

Fig. 5. Schematic of the FP interferometer.

According to Eqs. (4) and (5), the cavity length of the ultrashort FP interferometer could be calculated by measuring the reflective spectrum of the device.

3. EXPERIMENTAL RESULTS AND DISCUSSION

To corroborate the proposed FP interferometers, we fabricated a series of FP interferometers with different cavity lengths and measured the corresponding reflective spectra in our experiments. Figure 6 shows the whole experimental setup for the FP interferometers. The experimental setup consists of a broadband optical source (BBS), an optical circulator (OC), and an optical spectrum analyzer (OSA). Light from the optical source was injected into the FP interferometer through the optical circulator, and the reflected spectrum from the FP interferometer was monitored by the optical spectrum analyzer.

Using the above method, a series of FP interferometers with different cavity lengths is measured. Figure 7 shows the representative reflective spectra of the FP interferometers. According to the theoretical model of the two-beam interference, we can obtain that the cavity lengths of the FP interferometers in Fig. 7 are 7.57, 3.50, 2.91, and 1.18 μm, respectively. Cavity lengths of 7.57, 3.50, and 2.91 μm were calculated from the reflective spectra and Eqs. (4) and (5), but the cavity length of 1.18 μm was obtained by fitting the reflective spectrum according to the Eq. (1) with $R = 0.04$, $a_1 = a_2 = 0.05$, and $b = 0.11$ because the bandwidth of the optical source is smaller than the free spectrum range. It is possible for the proposed method to fabricate FP interferometers with submicrometer cavity lengths, although the submicrometer FP interferometer has not been shown limited by the small bandwidth of the optical source in our experiments. Owing to the smooth concave surfaces fabricated by the CO_2 laser, the fringe visibilities for the reflective spectra with cavity lengths of 7.57, 3.50, and 2.91 μm were more than 15 dBm, which is larger than most of those fabricated by a femtosecond laser or focused-ion beam. In addition, the cost of the CO_2 laser is far lower than that of a femtosecond laser or focused-ion beam.

The proposed ultrashort all-fiber FP interferometers could be used as a high-sensitivity strain sensor by embedding the FP interferometer into the smart structures to monitor the strain of the smart structures because the sensitivity of the strain sensor based on FP interferometer is inversely proportional to the cavity length. In addition, the proposed FP interferometer could also be used as an excellent filter for the large free spectral range. Therefore, the proposed method has great prospects in practical applications.

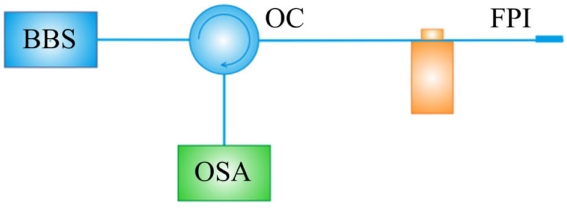

Fig. 6. Experimental setup for the FP interferometer.

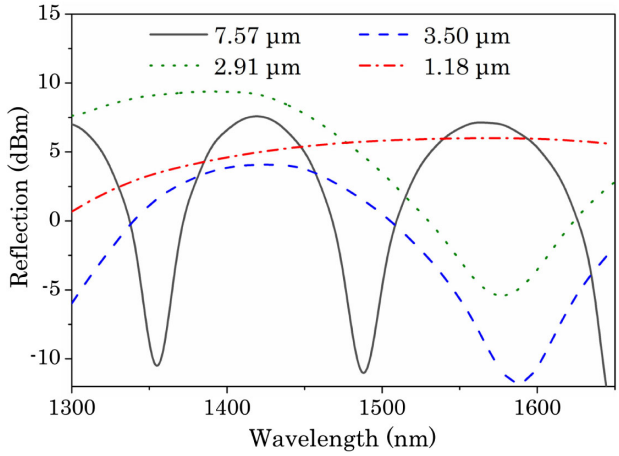

Fig. 7. Reflection spectra of the FP interferometers with different cavity lengths.

4. CONCLUSIONS

In conclusion, we have proposed and demonstrated experimentally a novel method to fabricate an ultrashort all-fiber Fabry–Perot interferometer. The proposed FP interferometer was constructed by splicing a standard SMF and another SMF with a concave surface, which was fabricated by focusing a CO_2 laser pulse on the end face of the SMF. By adjusting the parameters of the laser pulse and the relative position between the beam waist and the end face of the SMF, the parameters of the concave surface could be tailored flexibly. Experimental results showed that a series of grooves with the depth of 0.12–50 μm could be fabricated in our experimental setup. The proposed method provides a novel approach for ultrashort all-fiber FP interferometers. Moreover, the surface fabricated by the CO_2 laser was smooth, and the cost of the CO_2 laser is lower than that of a femtosecond laser or focused-ion beam. All these advantages indicate that the proposed FP interferometer has an ideal prospect in practical applications.

Funding. National Natural Science Foundation of China (11774209, 11804208); National Key Research and Development Program of China (2016YFA0301403); Key Research and Development Projects of Shanxi Province (201803D121065); Applied Basic Research Program of Shanxi Province (201801D221010); Shanxi 1331KS.

Disclosures. The authors declare no conflicts of interest.

REFERENCES

1. H. Nakstad and J. T. Kringlebotn, "Probing oil fields," Nat. Photonics **2**, 147–149 (2008).
2. M. Jones, "A sensitive issue," Nat. Photonics **2**, 153–154 (2008).
3. T. Zhu, D. Wu, M. Liu, and D. W. Duan, "In-line fiber optic interferometric sensors in single-mode fibers," Sensors **12**, 10430–10449 (2012).
4. M. R. Islam, M. M. Ali, M. Lai, K. Lim, and H. Ahmad, "Chronology of Fabry-Perot interferometer fiber-optic sensors and their applications: a review," Sensors **14**, 7451–7488 (2014).
5. Q. Zhang, P. Hao, X. Tian, and Y. Li, "High-visibility in-line fiber-optic optofluidic Fabry–Pérot cavity," Appl. Phys. Lett. **111**, 191102 (2017).

6. C. Zhang, Y. Gong, W. Zou, Y. Wu, Y. Rao, G. Peng, and X. Fan, "Microbubble-based fiber optofluidic interferometer for sensing," J. Lightwave Technol. **35**, 2514–2519 (2017).
7. J. Ma, J. Ju, L. Jin, W. Jin, and D. Wang, "Fiber-tip micro-cavity for temperature and transverse load sensing," Opt. Express **19**, 12418–12426 (2011).
8. A. Zhou, B. Qin, Z. Zhu, Y. Zhang, Z. Liu, J. Yang, and L. Yuan, "Hybrid structured fiber-optic Fabry-Perot interferometer for simultaneous measurement of strain and temperature," Opt. Lett. **39**, 5267–5270 (2014).
9. F. C. Favero, G. Bouwmans, V. Finazzi, J. Villatoro, and V. Pruneri, "Fabry-Perot interferometers built by photonic crystal fiber pressurization during fusion splicing," Opt. Lett. **36**, 4191−4193 (2011).
10. S. Liu, Y. Wang, C. Liao, G. Wang, Z. Li, Q. Wang, J. Zhou, K. Yang, X. Zhong, J. Zhao, and J. Tang, "High-sensitivity strain sensor based on in-fiber improved Fabry-Perot interferometer," Opt. Lett. **39**, 2121–2124 (2014).
11. Q. Zhang, T. Zhu, Y. Hou, and K. S. Chiang, "All-fiber vibration sensor based on a Fabry–Perot interferometer and a microstructure beam," J. Opt. Soc. Am. B **30**, 1211–1215 (2013).
12. C. Wu, Z. Liu, A. P. Zhang, B. O. Guan, and H. Y. Tam, "In-line open-cavity Fabry–Pérot interferometer formed by C-shaped fiber for temperature-insensitive refractive index sensing," Opt. Express **22**, 21757–21766 (2014).
13. P. Chen, X. Shu, and H. Cao, "Novel compact and low-cost ultraweak Fabry–Perot interferometer as a highly sensitive refractive index sensor," IEEE Photon. J. **9**, 7105810 (2017).
14. C. J. Alberts, S. deMan, J. W. Berenschot, V. J. Gadgil, M. C. Elwenspoek, and D. Iannuzzi, "Fiber-top refractometer," Meas. Sci. Technol. **20**, 034005 (2009).
15. C. Ma and A. Wang, "Optical fiber tip acoustic resonator for hydrogen sensing," Opt. Lett. **35**, 2043–2045 (2010).
16. W. Yuan, F. Wang, A. Savenko, D. H. Petersen, and O. Bang, "Note: optical fiber milled by focused ion beam and its application for Fabry-Pérot refractive index sensor," Rev. Sci. Instrum. **82**, 076103 (2011).
17. T. Wieduwilt, J. Dellith, F. Talkenberg, H. Bartelt, and M. A. Schmidt, "Reflectivity enhanced refractive index sensor based on a fiber-integrated Fabry-Perot microresonator," Opt. Express **22**, 25333–25346 (2014).
18. J. Li, F. Albri, R. R. J. Maier, W. Shu, J. Sun, D. P. Hand, and W. N. MacPherson, "A micro-machined optical fiber cantilever as a miniaturized pH sensor," IEEE Sens. J. **15**, 7221–7228 (2015).
19. Y. Zheng, L. H. Chen, J. Yang, R. Raghunandhan, X. Dong, P. L. So, and C. C. Chan, "Fiber optic Fabry–Perot optofluidic sensor with a focused ion beam ablated microslot for fast refractive index and magnetic field measurement," IEEE J. Sel. Top. Quantum Electron. **23**, 322 (2017).
20. P. A. R. Tafulo, P. A. S. Jorge, J. L. Santos, and O. Frazão, "Fabry–Pérot cavities based on chemical etching for high temperature and strain measurement," Opt. Commun. **285**, 1159–1162 (2012).
21. L. Yuan, J. Huang, X. Lan, H. Wang, L. Jiang, and H. Xiao, "All-in-fiber optofluidic sensor fabricated by femtosecond laser assisted chemical etching," Opt. Lett. **39**, 2358–2361 (2014).
22. Y. Rao, M. Deng, D. Duan, X. Yang, T. Zhu, and G. Cheng, "Micro Fabry-Perot interferometers in silica fibers machined by femtosecond laser," Opt. Express **15**, 14123–14128 (2007).
23. C. R. Liao, T. Y. Hu, and D. N. Wang, "Optical fiber Fabry-Perot interferometer cavity fabricated by femtosecond laser micromachining and fusion splicing for refractive index sensing," Opt. Express **20**, 22813–22818 (2012).
24. P. Chen and X. Shu, "Refractive-index-modified-dot Fabry-Perot fiber probe fabricated by femtosecond laser for high-temperature sensing," Opt. Express **26**, 5292–5299 (2018).
25. E. Cibula and D. Donlagic, "In-line short cavity Fabry-Perot strain sensor for quasi distributed measurement utilizing standard OTDR," Opt. Express **15**, 8719–8730 (2007).
26. Q. Shi, F. Lv, Z. Wang, L. Jin, J. J. Hu, Z. Liu, G. Kai, and X. Dong, "Environmentally stable Fabry-Pérot-type strain sensor based on hollow-core photonic bandgap fiber," IEEE Photon. Technol. Lett. **20**, 237–239 (2008).
27. M. Ramakrishnan, G. Rajan, Y. Semenova, and G. Farrell, "Overview of fiber optic sensor technologies for strain/temperature sensing applications in composite materials," Sensors **16**, 99–125 (2016).
28. J. J. Tian, Y. Jiao, Q. Fu, S. Ji, Z. Li, M. Quan, and Y. Yao, "A Fabry–Perot interferometer strain sensor based on concave-core photonic crystal fiber," J. Lightwave Technol. **36**, 1952–1958 (2018).
29. F. Laguarta, N. Lupon, and J. Armengol, "Optical glass polishing by controlled laser surface-heat treatment," Appl. Opt. **33**, 6508–6513 (1994).
30. K. M. Nowak, H. J. Baker, and D. R. Hall, "Efficient laser polishing of silica micro-optic components," Appl. Opt. **45**, 162–171 (2006).
31. D. K. Armani, T. J. Kippenberg, S. M. Spillane, and K. J. Vahala, "Efficient laser polishing of silica micro-optic components," Nature **421**, 925–928 (2003).
32. E. Mendez, K. M. Nowak, H. J. Baker, F. J. Villarreal, and D. R. Hall, "Localized CO_2 laser damage repair of fused silica optics," Appl. Opt. **45**, 5358–5367 (2006).
33. Q. Zhang, Z. Li, X. Tian, P. Hao, X. Wang, and Y. Li, "High-visibility, high-strength, rapid-response, in-fiber optofluidic sensor," J. Lightwave Technol. **36**, 2896–2902 (2018).